Journal of ELECTRICAL ENGINEERING, VOL 61. NO 7, 2010, 32-35

REAL TIME VISUALIZATION OF ALTERNATING MAGNETIC FIELDS USING 2-DIMENSIONAL INTEGRATED HALL SENSOR ARRAY

Jongwoo Jun* — Youngmin Park — Jinyi Lee*****

A visualization method of alternating magnetic fields done in real time with a high spatial resolution is proposed in this paper. 1024 Hall sensors are arrayed every 0.78 mm intervals in a 25×25 mm^2 area on a nickel-zinc ferrite wafer for measuring the magnetic field intensity. A 2.5~20 kHz alternating magnetic field could be visualized by using this AC-type magnetic camera. The inspection of surface cracks on aluminium alloy specimens using the distribution of the alternating magnetic field was done in order to verify this method.

Keywords: magnetic field, sensor array, non-destructive testing, magnetic flux leakage, sheet type induced current, crack inspection

1 INTRODUCTION

The damage and fracture of large magnitude constructions, such as aging aircraft, or nuclear power generation plants, occurs due to material degradation, cracking, and propagation. The initiation and propagation of cracks is due to (1) inclusions in the raw material, and (2) a weakening during operation caused by high temperatures, fatigue, and corrosion [1-2]. Currently cracks are detected by using pre-service inspections (PSI) and in-service inspections (ISI) and then maintained. Unfortunately aircraft cannot be maintained in-flight. Therefore, the ISI has to be done before take-off or after landing the aircraft in order to obtain high crack inspection ability. Aluminium alloy parts are used in aircraft in order to reduce the weight. The aluminium alloys are a paramagnetic metal. This allows electro-magnetic non-destructive testing (NDT) to be used for the ISI in aging aircraft.

A type of electro-magnetic NDT that provides magnetic images over a wide area is the magneto-optical eddy current imager (MOI); it uses the principle of the Faraday effect, [3]. When a polarized light beam is passed through a magneto-optical (MO) film, the polarization plane rotates due to the supplied magnetic field to the MO film. The induced current is distorted by a crack when a sheet-type current is induced in the specimen. The magnetic field is altered due to the above-mentioned distortion of the induced current, and so can be detected by the MO film. This method is useful for inspecting multi-site cracks in the riveting. However, because the resolution of the measured magnetic intensity of the MO film is 1 bit, the quantitative evaluation of cracks is difficult. In addition, the width of the magnetic domain and the saturated magnetization of the MO film vary according to changes in the temperature [4]. Therefore, the crack detection ability of this method is not stable.

The authors have been developing a magnetic field visualization system, named the magnetic camera [5]-[6]. Matrix-type Hall sensors arrays are used to visualize a magnetic field. There are two types of magnetic cameras, the DC-type and the AC-type, determined by their signal processing circuits. The DC-type magnetic camera is designed to visualize a magnetic field created by direct current or a permanent magnet. An alternating magnetic field with a low frequency of ~300 Hz can be visualized using the DC-type magnetic camera due to the high speed imaging circuits. The AC-type magnetic camera is designed to visualize a high frequency 0.3~20 kHz alternating magnetic field. In order to inspect cracks on paramagnetic metals like aluminium alloy, a sheet-type induced current (STIC) and an AC-type magnetic camera are used. Several artificial cracks were examined to verify the effectiveness of the AC-type magnetic camera used in this paper.

2 THE PRINCIPLES

The STIC consists of a coil, a core and a copper sheet, as shown in Fig. 1(a). An alternating magnetic field is developed in the core when an alternating current is applied to the coil. A current is induced in the copper sheet when the alternating magnetic field is passed through the core.

When the copper sheet is put onto a specimen, a STIC is induced in the specimen, as shown in Fig. 1(b). This STIC can be distorted due to a crack. The distribution of

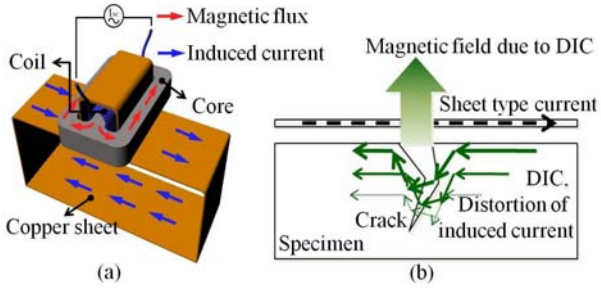

Fig. 1. The STIC principle: (a) - the sheet type induced current, (b) - the induced current in a specimen and the appearance of the magnetic field

* Research Center for Real Time NDT, Chosun University, ** Department of Control and Instrumentation Engineering, Graduate School of Chosun University, *** Department of Control and Instrumentation Robot Engineering, Chosun University, Gwangju, Republic of Korea; jinyilee@chosun.ac.kr

ISSN 1335-3632

the magnetic fields, including the distorted magnetic field, can be measured by using the arrayed Hall sensors in the magnetic camera.

1024 Hall sensors are arrayed at 0.78mm intervals in a 24.96×24.96 mm^2 nickel-zinc ferrite wafer, as shown in Fig. 2(a). As shown in Fig. 2(b), the input positive (+) pins of each Hall sensor in the column-direction are connected to each other and connected to switch SW-*i*(+). Here, *i* is the number of rows in the *m*×*n* matrix. The input negative (-) pins of each Hall sensor in the column-direction are also connected to each other and connected to switch SW-*i*(-). SW-*i*(+) and SW-*i*(-) are connected to the input power lines. The output positive (+) pins and the negative (-) pins of each Hall sensor in the row-direction are connected to each other and connected to signal lines *V*-*j*(+) and *V*-*j*(-), respectively. Where, *j* is the number of rows in the *m*×*n* matrix. In addition, the amplifiers, high-pass-filters (HPFs) and root-mean-square circuits (RMSs), having the same number as the n rows, are used for signal conditioning. By using this Hall sensor array and wiring, the distribution of the alternating magnetic field can be measured in the *m*×*n* matrix area. In other words, the alternating magnetic field amplitude at point (*i*, *j*) on the (*m*, *n*) matrix can be obtained by turning on SW-*i*(+) and SW-*i*(-), and measuring the signal line after *V*-*j*(+) and *V*-*j*(-). The root-mean-squared analogue

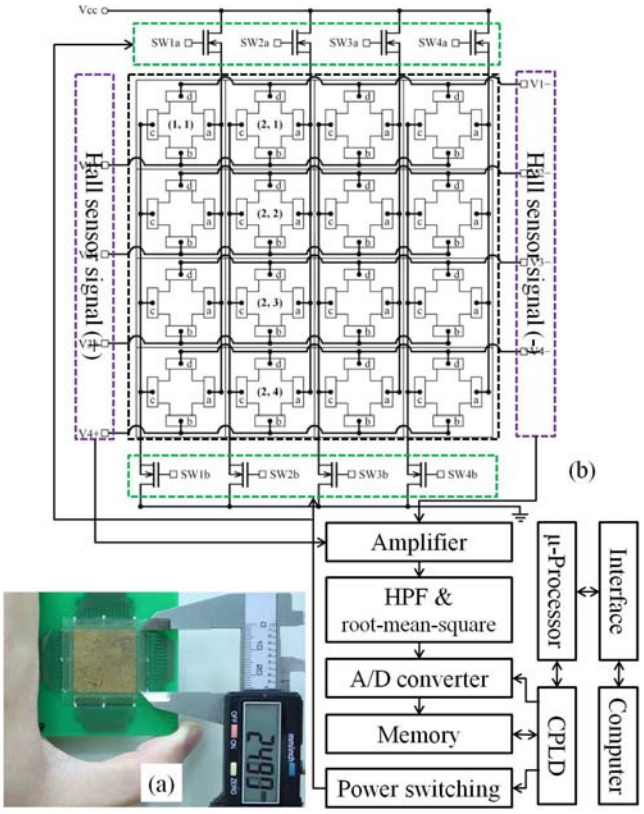

Fig. 2. The Hall sensor array matrix.

signals are digitized using analogue-to-digital convertors (ADCs), and temporarily stored in the memory. A complex programmable logic device (CPLD) controls the ADCs, memory, and power switching for SW-*m*. The resulting digitized alternating magnetic field amplitude is input to the computer interface, stored, calculated and displayed.

By using the above-mentioned STIC and Hall sensor array, the distorted alternating magnetic field due to the existence of a crack can be visualized without using conventional scanning equipment.

3 THE EXPERIMENT AND DISCUSSIONS

Figure 3 and Table 1 show the shape and size of each crack on the surface of the aluminium alloy specimens (Al7075). A 10 mm artificial crack was introduced to the centre of each specimen using electro-discharge-machining (EDM). The sectional shapes of the cracks are rectangular, triangular, elliptical, and stepped.

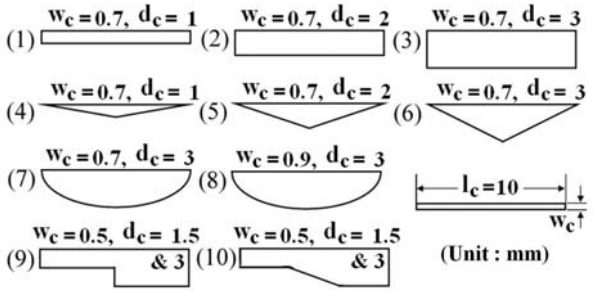

Fig. 3. The shapes and sizes of the cracks

Table 1. The size of each crack (unit: mm)

Crack No	Length	Width	Depth	Crack angle
1	10	0.7	1	90°
2	10	0.7	2	90°
3	10	0.7	3	90°
4	10	0.7	1	11.3°
5	10	0.7	2	21.8°
6	10	0.7	3	30.96°
7	10	0.7	3	61.9°
8	10	0.9	3	61.9°
9	10	0.5	1.5&3	90°
10	10	0.5	1.5&3	90°

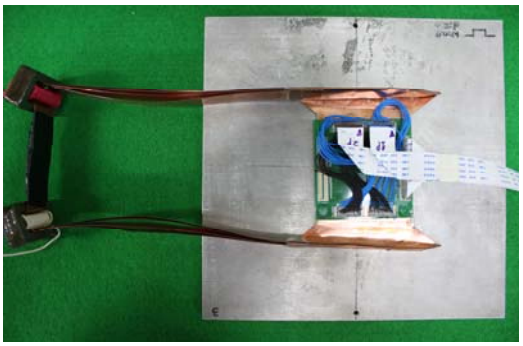

Fig. 4. The STIC and Hall sensor array on a specimen

Figure 4 shows the STIC and the Hall sensor array on a specimen used in this paper. The 0.1 mm thick copper sheet has a 64×64 mm^2 of effective STIC area. Two figure 8 shaped 25×40×11 mm^3 silicon steel cores, with two 30×5 mm^2 holes are used to induce the current in the STIC. 34 turns of coils are wound around each core centre. An alternating current (2.5 A, rms) at 5, 10 and 20 kHz are applied to each coil. The Hall sensor array, with the effective area of 24.96×24.96 mm^2, is positioned on a 64×64 mm^2 printed circuit board (PCB). The Hall voltages are amplified by 72 dB. HPFs with a 1.59 kHz cut-off frequency are used to improve the signal-to-noise ratio.

The obtained RMS distribution of the alternating magnetic field (V_R) and the processed images ($\partial V_R/\partial x$) using the developed AC-type magnetic camera, as expressed in Fig.5. $\partial V_R/\partial x$ is calculated by:

$$\frac{\partial V_R}{\partial x} \approx V_R(i,j) - V_R(i+1,j) \qquad (1)$$

As shown in Fig. 5(a), there are two large peaks located around the two crack tips of specimen No.3 in the V_R image. As mentioned, all of the cracks used in this paper have a length of 10mm. The peak-to-peak distance in the V_R image is approximately the same as the length of the rectangular crack. The $\partial V_R/\partial x$ image, shown in Fig. 5(b), shows the row-directional gradient of the V_R. The two peaks in the V_R image appear on the crack tips, as indicated by the dotted arrow. We can see that the 12.5mm peak-to-peak distance, indicated by the solid arrow in Fig. 5(b) and referred to as the L_P, has a greater length than the real crack length of 10mm. This is because the two peaks appear outside of the crack tips in the $\partial V_R/\partial x$ image.

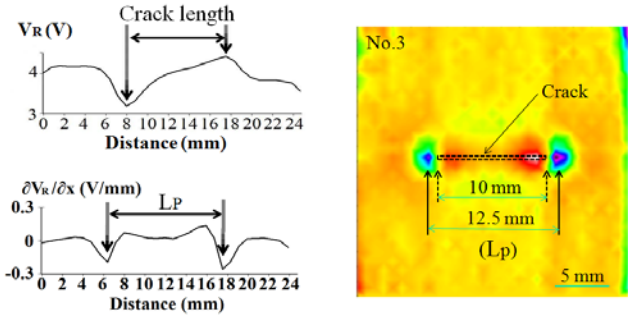

(a) (b)

Fig. 5. The distribution of the magnetic field and the processed image of the No.3 crack at 10 kHz: (a) – section view of V_R, (b) – $\partial V_R/\partial x$ image

Figure 6 shows the $\partial V_R/\partial x$ image with a 10 kHz STIC. Corresponding to the increasing crack depth, the peak value increases and the contrast is clearer than that found for the smaller depth in the same crack shape. Also, as shown in Nos.9 and 10, which have the stepped cracks, the width of the peak at the deeper crack tip is larger than the one at the shallow crack tip. Therefore, the entire shape of this type of crack can be estimated by using the $\partial V_R/\partial x$ image. In the case of the rectangular cracks, Nos.1, 2 and 3, not only the peak-distance L_P, shown by the solid arrow in Fig. 5(b), but also the crack length, shown as the dotted arrow in Fig. 5(b), can be estimated. However, in the case of triangular (Nos.4, 5 and 6) and elliptical cracks (Nos.7 and 8), only the L_P can be known. Therefore, the peak-distance L_P is the most useful factor used to estimate the length of a crack seen in a $\partial V_R/\partial x$ image.

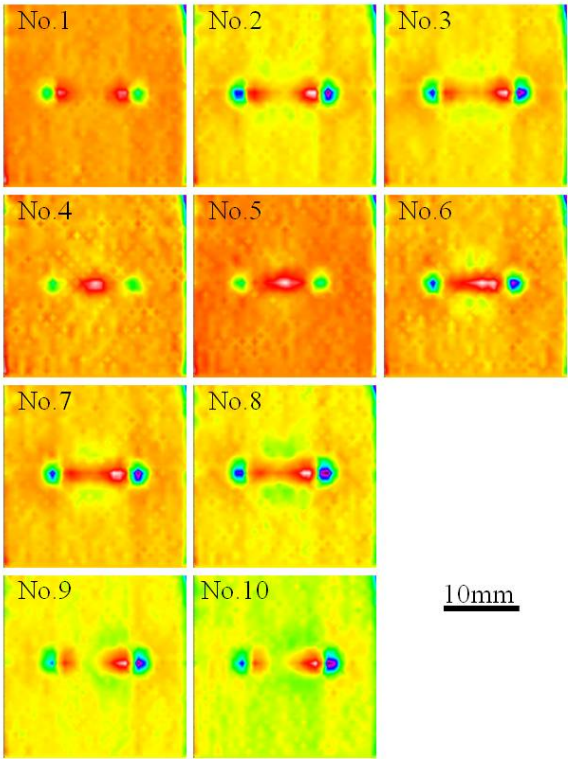

Fig. 6. The $\partial V_R/\partial x$ image from a 10 kHz STIC

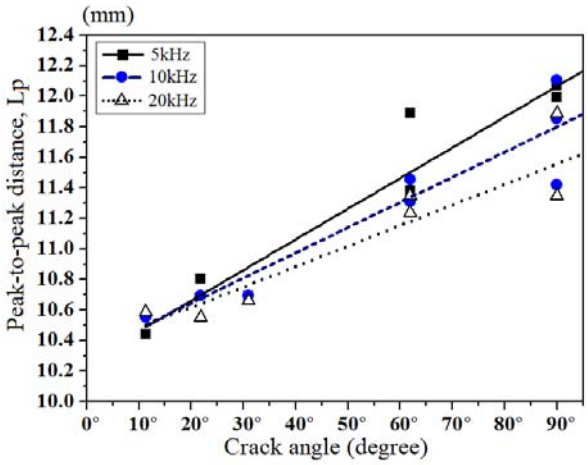

Fig. 7. The relationship between the peak-to-peak distance (L_P) in the $\partial V_R/\partial x$ image and the crack-angle

Figure 7 shows the relationship between the crack-angle, which expresses the angle between the surface of the specimen and the tip-side in the depth direction, and the peak-to-peak distance L_P. The L_P increased propor-

tionally to the crack-angle. This phenomena means that the distortion of the induced current on the crack tips is dependent on the crack shape.

On the other hand, the current density for the depth of t, J_t, can be expressed using (2) and (3) [7].

$$J_t = e^{-t/\delta} J_S, \quad \delta = \frac{1}{\sqrt{\pi f \mu \sigma}} \qquad (2), (3)$$

Here, J_S is the current density on the surface of specimen. The skin depth δ is the depth where J_t decreases to 36.79 % of J_S. Symbols, f, μ and σ are the frequency, permeability and conductivity, respectively. As shown in (2) and (3), if the frequency increases, the skin depth decreases.

Therefore, the current density is concentrated near the surface at high frequencies. As a result, the L_P for a high frequency STIC is smaller than the L_P for a low frequency, as shown in Fig. 7.

Figure 8 shows the relationship between the crack volume and the integrated absolute values of the magnetic intensity for each $\partial V_R/\partial x$ magnetic image (magnetic-integral) as expressed by

$$\left.\frac{\partial V_R}{\partial x}\right|_{TOTAL} \approx \sum_{i=1}^{m-1}\sum_{j=1}^{n}\left|\frac{\partial V_R(i,j)}{\partial x}\right|, \qquad (4)$$

where m and n are the column and row numbers of the Hall sensor array, respectively, in this case it was 32. The magnetic-integral increases proportionally to the crack volume; the volume of the crack can be estimated by using this magnetic-integral, as shown in Fig. 8.

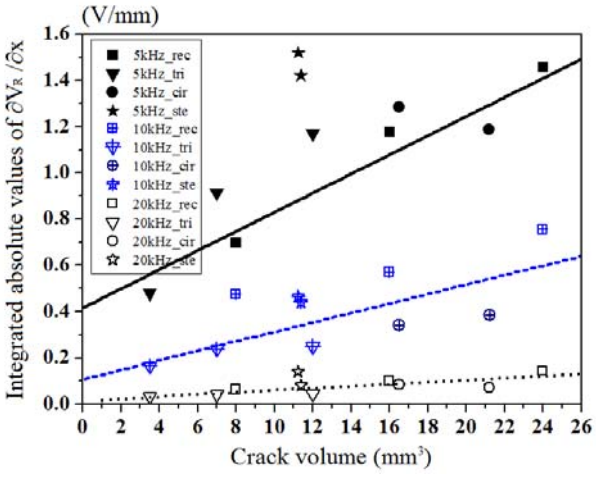

Fig. 8. The relationship between the crack volume and the integrated absolute values of $\partial V_R/\partial x$

4 CONCLUSIONS

An alternative magnetic field visualization system, entitled an AC-type magnetic camera, useful for inspecting cracks on paramagnetic metal plates was proposed in this paper. The distortion of a magnetic field around a crack was induced by using a sheet type induced current. The distribution of the magnetic field, including the crack information, was measured using 1024 Hall sensors arrayed in a matrix, with a 0.78 mm spatial resolution. Cracks with a length of 10mm, a depth of 1mm and a width of 1mm could be detected. In addition, the shape of these cracks could be predicted and the volume of the cracks could be estimated.

Acknowledgement

This work was supported by the Korea Science and Engineering Foundation (KOSEF) grant funded by the Korean government (MEST) (grant code: 2008-06003). Also this research was supported by the MKE (The Ministry of Knowledge Economy), Korea, under the ITRC (Information Technology Research Centre) support program supervised by the NIPA (National IT Industry Promotion Agency) (NIPA-2010-C1090-1021-0013). We are grateful of support.

REFERENCES

[1] GORANSON, U. G.: Damage tolerance-facts and fictions: Proc. 17th Int. Conf. in Aeronautical Fatigue Sweden, Vol. 1 (1993), 3-105

[2] HWANG, D.: Damage tolerance design and prediction of fatigue life in aircraft structure, KSME Int. Journal, Vol. 35 (1995), 468-480

[3] THOME, D. K. – FITZPATRICK, G. L. – SKAUGSET, R. L. – SHIH, W. C. L.: Aircraft corrosion and crack inspection using advanced magneto-optic imaging technology, Proceedings of SPIE, vol. 2945 (1996), 365-373

[4] LEE, J. Y. – WANG, R. L. – SHOJI, T. S. – HONG, S. P.: Non-destructive Testing in the High-temperature Regime by Using a Magneto-optical Film, NDT&E International 41 (2008), 420-426

[5] JUN, J. W. – HWANG, J. S. – KIM, K. J. – OGAWA, K. – LEE, J. Y.: Development of Signal Processing Circuit of a Magnetic Camera for the NDT of a Paramagnetic Material, Key Engineering Materials, Vol. 353-358 (2007), 2379-2382

[6] HWANG, J. S. – KIM, J. M. – LEE, J. Y.: Magnetic Images of Surface Crack on Heated Specimen Using an Area-type Magnetic Camera with High Spatial Resolution, Instrumentation and Measurement Technology Conference, I2MTC '09. IEEE Proceedings, (2009), 1546-1551

[7] PANAITOV, J. – KRAUSE, H. J. – ZHANG, Y.: Pulsed Eddy Current Transient Technique with HTS SQUID Magnetometer for Non-destructive Evaluation, Physics C, 372-376 (2002), 278-281

Received 30 September 2010